nuclear fusion
IAEA

PAPER

Determination of radial electric field from Pfirsch–Schlüter flows in the HSX stellarator

To cite this article: S.T.A. Kumar *et al* 2017 *Nucl. Fusion* **57** 036030

View the article online for updates and enhancements.

Related content

- Radial electric field and ion parallel flow in the quasi-symmetric and Mirror configurations of HSX
S T A Kumar, T J Dobbins, J N Talmadge et al.
- Measurement and calculation of the radial electric field in the stellarator W7-AS
J Baldzuhn, M Kick, H Maassberg et al.
- Intrinsic plasma rotation and Reynolds stress at the plasma edge in the HSX stellarator
R.S. Wilcox, J.N. Talmadge, D.T. Anderson et al.

Recent citations

- Effect of the Pfirsch–Schlüter flow on the inboard/outboard asymmetry of the toroidal flow in LHD
Y. Yamamoto *et al*
- Investigation of the neoclassical ambipolar electric field in ion-root plasmas on W7-X
N. Pablant *et al*
- The role of neutral friction in governing parallel flows in the HSX stellarator
T.J. Dobbins *et al*

IOP ebooks™

Bringing together innovative digital publishing with leading authors from the global scientific community.

Start exploring the collection–download the first chapter of every title for free.

This content was downloaded from IP address 128.104.46.206 on 10/06/2020 at 16:22

IOP Publishing | International Atomic Energy Agency Nuclear Fusion

Nucl. Fusion **57** (2017) 036030 (6pp) doi:10.1088/1741-4326/aa52a2

Determination of radial electric field from Pfirsch–Schlüter flows in the HSX stellarator

S.T.A. Kumar, J.N. Talmadge, T.J. Dobbins, F.S.B. Anderson, K.M. Likin and D.T. Anderson

Department of Electrical and Computer Engineering, HSX Plasma Laboratory, University of Wisconsin-Madison, Madison, WI, United States of America

E-mail: stkumar@wisc.edu

Received 5 July 2016, revised 17 November 2016
Accepted for publication 6 December 2016
Published 6 February 2017

Abstract

Inboard/outboard asymmetry in the impurity ion parallel flow is observed in the HSX stellarator using charge exchange recombination spectroscopy (CHERS). This observation shows the presence of counter-streaming Pfirsch–Schlüter flow predicted by neoclassical theory. The asymmetry of the flow is used to calculate the magnitude and direction of the radial electric field (E_r), as well as the mean flow, using computed magnetic geometry factors. This method enables calculation of E_r near the core of the HSX plasma where the E_r obtained from the radial force balance equation has large uncertainties due to the relatively large width of the diagnostic neutral beam with respect to the plasma minor radius.

Keywords: stellarator, radial electric field, Pfirsch–Schlüter flows

(Some figures may appear in colour only in the online journal)

1. Introduction

The radial electric field (E_r) plays an important role in the plasma confinement in stellarators. It significantly affects the neoclassical particle, impurity and heat transport. Non-ambipolar transport in stellarators generates the E_r, which can take one of multiple stable values at which the ambipolarity condition is satisfied. It is well known that the increased neoclassical transport in the low collisionality regime in stellarators (called $1/\nu$ transport) is greatly reduced if a large E_r is present [1]. Also, a positive E_r near the plasma core could expel impurities [2]. A large E_r can also lead to changes in the MHD equilibrium configuration by its effect on the bootstrap current [3, 4]. An accurate measurement of E_r is therefore important to understand the transport properties of a stellarator device.

The radial electric field in fusion devices is usually obtained from impurity ion flows or from the electric potential profile measured by a heavy-ion beam probe. Previously, the E_r in the HSX stellarator has been obtained from the radial force balance equation, using the measured C^{+6} impurity ion flows [5, 6]. This technique involves measuring both poloidal and toroidal flows accurately and simultaneously. Because the diagnostic neutral beam width can be comparable to the plasma diameter near the core, poloidal flow measurements in this region are subjected to large uncertainties. This is because the beam intersection with the optical sight-lines cut through regions with different velocity vectors. However, by observing the carbon emission parallel to the magnetic field at the inboard and outboard side of the torus (or any two points on a flux surface where large flow variation is expected), it is possible to calculate the radial electric field and the mean ion flow from the Pfirsch–Schlüter effect.

The Pfirsch–Schlüter flows manifest in the form of an inboard/outboard asymmetry in the measured parallel flows. Recently, Pfirsch–Schlüter flows deduced from such asymmetry have been used to verify the compressible and incompressible nature of ion flows in the TJ-II stellarator [7, 8]. Measurements of the Pfirsch–Schlüter current in HSX using magnetic coils agreed well with a neoclassical calculation that assumed incompressibility [9]. The measurements confirmed the helical nature of the Pfirsch–Schlüter current and its reduced magnitude because of the high effective transform. The ion and electron flow both depend on the pressure gradient and the electric field. However, when flows are summed (as in the measurement of Pfirsch–Schlüter current), the

 © 2017 IAEA, Vienna Printed in the UK

electric field drops out. Results presented in this paper utilize the asymmetry of the observed ion flow to calculate the magnitude and direction of the radial electric field (E_r), as well as the mean flow, using computed magnetic geometry factors.

The rest of the paper is organized as follows: in section 2, a theoretical background of the Pfirsch–Schlüter flows and the derivation of the E_r are presented. The experimental techniques and the results are presented in section 3. Comparison of the experimental results with neoclassical calculations are also presented in this section. Section 4 discusses the results in the light of similar measurements made in other machines and presents possible reasons for the discrepancy between experiment and neoclassical calculations. Conclusions are given in section 5.

2. Theoretical background

The Pfirsch–Schlüter flows are flows parallel to the magnetic field lines in a toroidal plasma that arise due to incompressibility. For ions, the incompressibility leads to the condition that

$$\nabla \cdot (\vec{v}_{\perp i} + \vec{v}_{\parallel i}) = 0 \tag{1}$$

where $\vec{v}_{\perp i}$ and $\vec{v}_{\parallel i}$ are ion flow velocities in the perpendicular and parallel directions to the magnetic field line respectively. There is no external momentum injection in the HSX plasma, so all flows described in this paper are intrinsic. Perpendicular flows are generated by the radial electric field (E_r) and the ion pressure gradient (∇P_i).

$$\vec{v}_{\perp i} = \frac{\vec{E}_r \times \vec{B}}{B^2} - \frac{\nabla P_i \times \vec{B}}{e n_i Z_i B^2} = -\left(\frac{\mathrm{d}\phi}{\mathrm{d}\psi} + \frac{1}{e n_i Z_i}\frac{\mathrm{d}P_i}{\mathrm{d}\psi}\right)\left(\frac{\nabla\psi \times \vec{B}}{B^2}\right) \tag{2}$$

where ϕ is the electrostatic potential and ψ is the toroidal flux. The parallel ion flow at any location in the plasma is given by,

$$\vec{v}_{\parallel i} = \vec{v}_{\mathrm{BS}} + \vec{v}_{\mathrm{PS}} \tag{3}$$

where the 'bootstrap' portion of the flow ($\vec{v}_{\mathrm{BS}}$) is a flux surface quantity (divergence-free) and the Pfirsch–Schlüter flow ($\vec{v}_{\mathrm{PS}}$) varies over a flux surface such that the flux-surface average is zero. Using equations (1), (2) and (3), the Pfirsch–Schlüter flow can be written as [10, 11]

$$\vec{v}_{\mathrm{PS}} = \left(\frac{\mathrm{d}\phi}{\mathrm{d}\psi} + \frac{1}{e n_i Z_i}\frac{\mathrm{d}P_i}{\mathrm{d}\psi}\right) h\vec{B} \tag{4}$$

where h is a geometrical factor, which is defined by

$$\vec{B} \cdot \nabla h = -2\frac{(\vec{B} \times \nabla B) \cdot \nabla\psi}{B^3}, \langle hB^2 \rangle = 0. \tag{5}$$

In HSX, the ions are cold (~50 eV) and the ion temperature profile is relatively flat throughout most of the plasma radius (figure 1(*d*)). Therefore, the pressure gradient contribution to the Pfirsch–Schlüter flow is small compared to the electric field, and can be neglected. Considering only the scalar quantity along the direction of the magnetic field,

$$v_{\mathrm{PS}} = \frac{\mathrm{d}\phi}{\mathrm{d}\psi} hB. \tag{6}$$

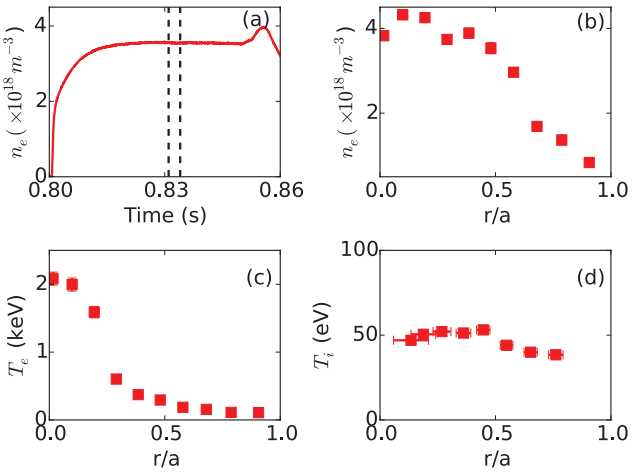

Figure 1. (*a*) Line averaged electron density measured by an interferometer, (*b*) radial profile of electron density and (*c*) electron temperature measured at $t = 0.82$ s using Thomson scattering diagnostic, and (*d*) C^{+6} ion temperature measured using CHERS. Vertical dashed lines on (*a*) represent start and end times of the diagnostic neutral beam used for CHERS measurements. Data are averaged over nine similar discharges used for the flow analysis.

Therefore, the flux surface constant, $\mathrm{d}\phi/\mathrm{d}\psi$, can be written as,

$$\frac{\mathrm{d}\phi}{\mathrm{d}\psi} = \frac{v_{\mathrm{PS}}}{hB} = \frac{v_{\parallel i} - v_{\mathrm{BS}}}{hB}. \tag{7}$$

Here, $v_{\parallel i}$ can be obtained from CHERS flow measurements, the hB factor at the measurement location can be calculated and the v_{BS} can be obtained from two point flow measurements on a flux surface as explained below. The flux surface constant, $\mathrm{d}\phi/\mathrm{d}\psi$, can thus be determined from the Pfirsch–Schlüter flows.

3. Experimental results and analysis

Experiments are made in the HSX stellarator, which is a medium sized stellarator (average minor radius = 0.12 m, average major radius = 1.2 m) that is optimized for neoclassical transport [12, 13]. For the results reported in this paper, plasmas heated using a 100 kW electron cyclotron heating system have been used. Measurements are made for the standard quasi-helically symmetric (QHS) magnetic geometry with an on-axis magnetic field of 1 T. The core electron density and temperature measured using a Thomson scattering diagnostic are $\sim 4 \times 10^{18}$ m^{-3} and ~2 keV respectively (figures 1(*b*) and (*c*)).

Flow measurements are made using charge exchange recombination spectroscopy (CHERS). A 30 keV, 3 ms, 4 A hydrogen diagnostic neutral beam is injected radially into the plasma during the stationary phase of the discharge, as shown in figure 1(*a*). The CVI emission at 529.1 nm ($n = 8$–7 transition) is measured using two Czerny–Turner spectrometers equipped with electron multiplying CCD cameras that capture a series of images during the plasma discharge. Each image consists of emission averaged over ~5 ms duration. The image captured before the beam is fired is subtracted from the image obtained when the beam is fired to get the beam

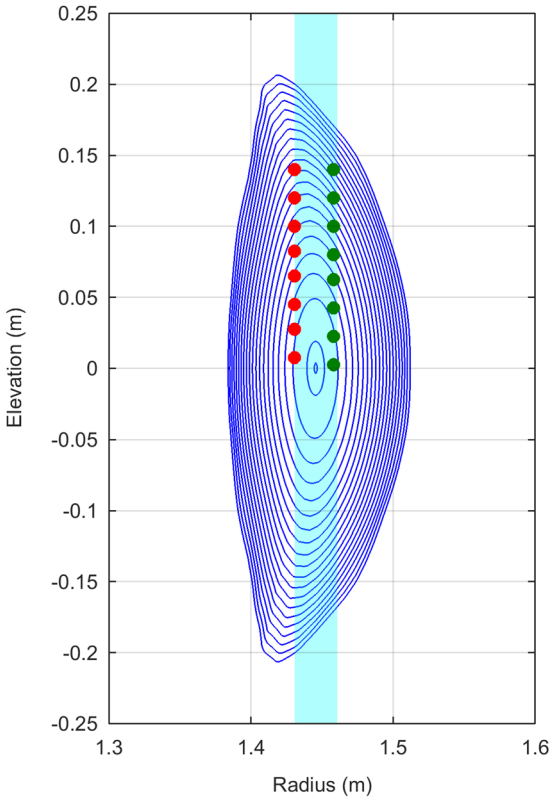

Figure 2. Poloidal cross-section of HSX magnetic flux surfaces where CHERS measurements are made. The vertical shaded band represents the approximate $1/e$ width of the neutral beam injected from the top as it traverses the plasma. Red and green dots represent inboard and outboard measurement locations respectively (spot radius 1.5 mm). For clarity, the spot size in the figure is enlarged by a factor of three.

induced charge-exchange emission (see [5] for details). Since boronization is used for wall conditioning in HSX, the carbon signal level in a pure hydrogen plasma is too low to be used for CHERS. Therefore, for the results presented in this paper, methane is used as the working gas instead of hydrogen. Emission spectra from nine similar discharges are averaged for the analysis.

For this experiment, the toroidal view (due to the helical axis of the device, the views are only approximately toroidal in HSX) of the HSX CHERS diagnostic that measured flows at radial locations along the beam axis (see figure 1 of [6]) has been modified to view the inboard and outboard side of the beam axis, within the beam width, as shown in figure 2. The collection optics of the diagnostic has also been modified to make the views focused at the beam rather than using the larger diameter collimated sight-lines used in the past. These modifications reduced the spot size radius from 10 to 1.5 mm and improved spatial localization. The inboard and outboard locations are separated from the beam axis by about 1 cm on each side. The parallel ion velocity ($\vec{v}_{\|i}$) is obtained from the measured toroidal flows ($\vec{v}_{\rm tor}$) by accounting for the small angles (θ) the sight-lines make with the magnetic field vector [$\vec{v}_{\|i} = \vec{v}_{\rm tor}/\cos(\theta)$]. The hB factor at these locations is calculated by solving the magnetic differential equations (equation (5)) for the QHS geometry of HSX following [10, 11]. These

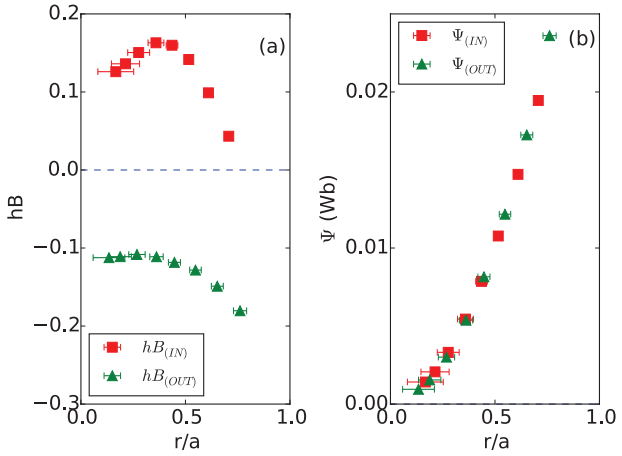

Figure 3. The hB factor and the toroidal flux (ψ) calculated for the QHS geometry at the measurement locations. The values shown are the weighted-average along the sight-line within the beam width. Horizontal error bars indicate the radial spread of each sight-line.

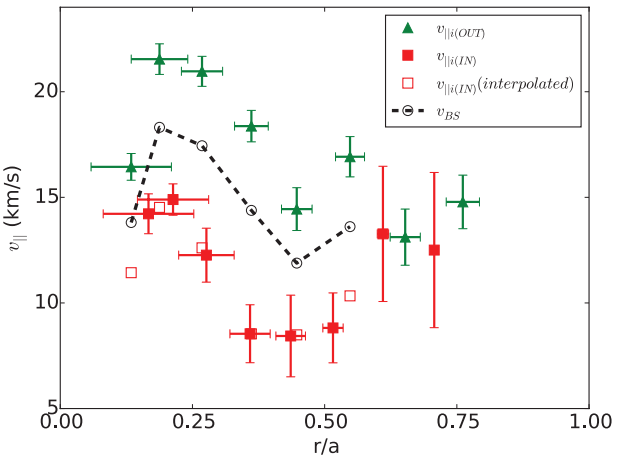

Figure 4. Parallel flow velocity obtained from CHERS at the inboard (solid red squares) and outboard (solid green squares) locations. The open red squares are the interpolated values on the inboard side. Also plotted is the bootstrap contribution to the flow ($v_{\rm BS}$). Larger vertical error bars for r/a > 0.6 for the inboard side measurements are due to lower signal levels. Therefore, $v_{\rm BS}$ could not be calculated at these locations.

values are plotted in figure 3. A synthetic diagnostic for beam emission spectroscopy is used to account for the finite beam width by taking the weighted average of these variables along the measurement sight-line within the beam width [14].

Figure 4 shows the parallel flows obtained from CHERS as a function of normalized radius for the inboard (solid red) and outboard (solid green) locations. Inboard–outboard asymmetry in the parallel flow is apparent from the measurements. The bootstrap flow, $v_{\rm BS}$, is calculated from the measured inboard/outboard flows using the condition that the $\mathrm{d}\phi/\mathrm{d}\psi$ and $v_{\rm BS}$ on both sides of the same flux surface (same r/a values, where r/a is the square root of the normalized toroidal flux) are the same. Therefore, for inboard and outboard measurements on a flux surface,

$$\frac{v_{\|i(IN)} - v_{\rm BS}}{(hB)_{(IN)}} = \frac{v_{\|i(OUT)} - v_{\rm BS}}{(hB)_{(OUT)}} \qquad (8)$$

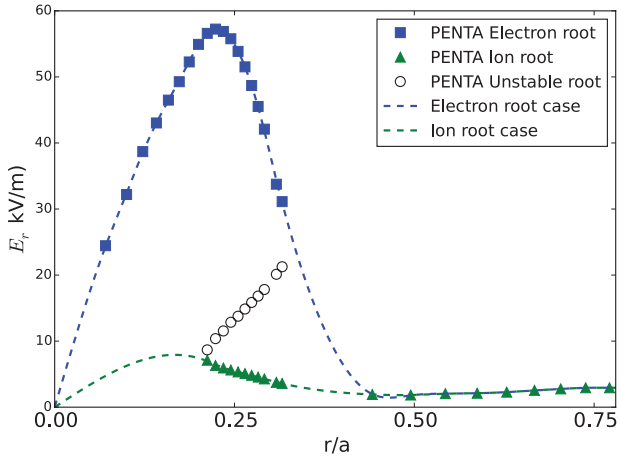

Figure 5. Neoclassical values for E_r calculated by the PENTA code (points). Dashed lines are two possible scenarios selected from the PENTA results, which are cubic smoothing splines of the selected data sets with a constraint, $E_{r(r/a=0)} = 0$.

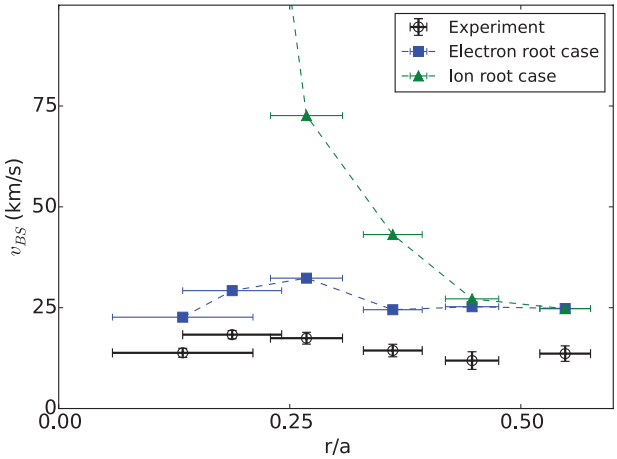

Figure 6. The bootstrap flow (v_{BS}) obtained from the Pfirsch–Schlüter flows compared to the neoclassical calculations. The PENTA profiles are the weighted average over the line of sight. Horizontal error bars indicate the radial spread of each sight-line.

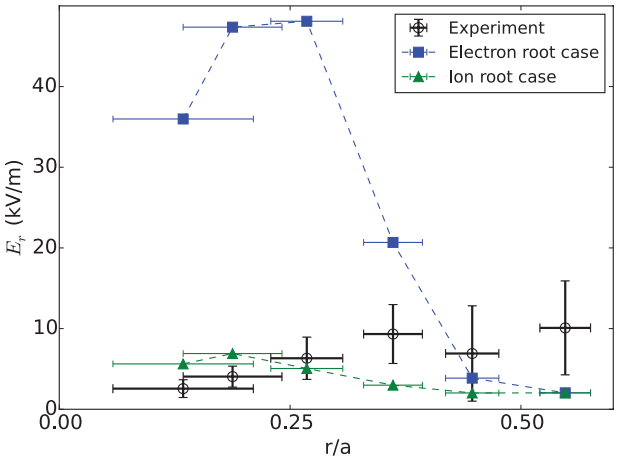

Figure 7. The radial electric field obtained from the Pfirsch–Schlüter flows compared to the PENTA calculated E_r. The PENTA profiles are the weighted average over the line of sight. Horizontal error bars indicate the radial spread of each sight-line.

where subscripts '*IN*' and '*OUT*' represent inboard and outboard measurement locations. The measurement locations are not exactly at the same r/a values on either side as can be seen from figures 3 and 4. To align the data points on the same flux surface, the inboard data points are interpolated as shown by the open red squares in figure 4. We assumed $v_{\parallel(r/a=0)} = 0$ to obtain the innermost data point. The solid green points on the outboard side and the open red points on the inboard side are used to obtain $\mathrm{d}\phi/\mathrm{d}\psi$ and v_{BS}. The calculated v_{BS} is between the inboard and outboard flows as shown in figure 4. The Pfirsch–Schlüter flows are therefore counter-streaming: parallel to the magnetic field lines in the outboard region and anti-parallel to the field lines at the inboard region as expected (from figure 3(*a*)) for a positive radial electric field.

Neoclassical calculations of the flows and the electric field, for the experimental parameters reported here, are done using the PENTA code [15, 16]. Along with the electron and ion temperatures and densities, the fractional abundance of carbon impurity calculated using ADAS [17] and scaled for methane (CH_4) proportion, is used in the calculation. The PENTA code uses a radial coordinate system based on the toroidal magnetic flux ($r_{\mathrm{PENTA}} = \sqrt{\psi/\pi B_T}$, where ψ and B_T are the toroidal magnetic flux and toroidal magnetic field respectively). The calculated value of $\mathrm{d}\phi/\mathrm{d}\psi$ based on the flow asymmetry can be converted into a PENTA variable $E_r = -\mathrm{d}\phi/\mathrm{d}r_{\mathrm{PENTA}}$ by multiplying by a factor $f = -\mathrm{d}\psi/\mathrm{d}r_{\mathrm{PENTA}} = -2\sqrt{\pi B_T \psi}$. The toroidal flux, ψ, calculated at the measurement location is given in figure 3(*b*). The parallel ion flow calculated by the PENTA code ($v_{\parallel}\vec{B}/B^2$) can be directly compared to the v_{BS} obtained from Pfirsch–Schlüter flows as $B = 1$ T.

The E_r calculated by the PENTA code is given in figure 5. It can be seen that there are locations where multiple solutions ('roots') exist; electron root, ion root and the unstable root. In general, if electrons are preferentially heated as in the case of HSX plasmas, the electron radial flux can exceed that of ions and the electron root is attained [18]. From the PENTA calculated electric field values, two possible scenarios for the radial E_r profile have been selected for comparison with experiment, the electron root case and the ion root case, as shown in figure 5. As the name suggests, the electron root case takes electron root E_r values and the ion root case takes ion root E_r values wherever multiple solutions exist. For both cases, $E_{r(r/a=0)} = 0$ is imposed and radial profiles are formed by fitting the respective data sets with cubic spline (dashed lines in figure 5). The weighted average of E_r over the line of sight is then calculated. A similar procedure was applied to ion flow velocities calculated by PENTA.

Figures 6 and 7 show a comparison of experimental values of velocity and radial electric field to the two cases selected from the PENTA results. It can be seen that the experimental flow velocities are slightly lower, but the profile shape qualitatively agrees with the PENTA electron root case profile. However, the experimental E_r exhibits a large discrepancy with the electron root case, both in magnitude and profile shape. In the core region, the experimental E_r agrees better with the PENTA ion root case.

4. Discussion

Previously, poloidal asymmetry in the parallel flow has been observed in the H-mode pedestal region of tokamaks where a large ion pressure gradient exists [20, 21]. These observations are consistent with the expectation that the impurity flows could become compressible in the steep gradient region. Flow compressibility in this case arises due to the redistribution of impurity ions resulting from the parallel friction caused by large ion diamagnetic velocities [22]. In a different scenario, experiments from the TJ-II stellarator showed, by analyzing the flow asymmetry and the Pfirsch–Schlüter component of the flow, that ion flows are incompressible in a low density electron cyclotron heated plasma [8], but a compressible flow variation occurs at higher density in ion-root neutral beam heated plasmas [7]. However, results reported in this paper are from a low density electron cyclotron heated plasma with negligible ion pressure gradients. Also, as mentioned in the introduction, measurements of the Pfirsch–Schlüter currents in HSX using magnetic coils agreed well with a neoclassical calculation that assumed incompressibility [9]. Another assumption used in our analysis is that the electric potential on a flux surface is constant. A variation of electrostatic potential of several tens of Volts on a flux surface has been measured using Langmuir probes at the edge of TJ-II plasma [23]. The effect of such a variation in the impurity dynamics has also been studied recently [24]. However, our measurements are near the core to mid radius of the plasma and calculations with the SFINCS code [25] for the neoclassically optimized QHS configuration used for the current experiment shows negligible ($\sim$1 V) variation.

The reason for the discrepancy between experimental results and the PENTA code calculations is not understood at present. Investigations are underway to examine the role of some of the assumptions used in the PENTA code that may be invalid for the HSX plasma. For example, the PENTA code neglects the variation of electrostatic potential energy over the radial excursion of the ion orbit (called 'mono-energetic' assumption) that breaks down at the helical resonance [19]. Since the large positive electric field calculated by the PENTA code is the result of the increased ion radial flux at the helical resonance, correcting for the mono-energetic assumption may result in a lower electron-root E_r. We are using the SFINCS code that does not have the mono-energetic ion assumption, to benchmark the PENTA code results. It could also be possible that the bootstrap ion flow evolves throughout the discharge, whereas the radial electric field reaches a steady state early in the discharge, as indicated by the previous measurements of bootstrap and Pfirsch–Schlüter current [9]. Evolution of the bootstrap flow may bring the experimental flow values to the steady-state values calculated by the PENTA code. This topic is left to future work.

5. Conclusions

In summary, the counter-streaming Pfirsch–Schlüter flows have been obtained from the toroidal flows measured using the CHERS system in the HSX stellarator. These measurements enabled calculation of the radial electric field in the core region of the plasma where poloidal flow measurements have large uncertainties and the E_r calculation from radial force balance equation is difficult. The Pfirsch–Schlüter flow method presented in this paper gives a way to obtain E_r from toroidal flow measurements, instead of estimating it from the radial force balance equation. This method is especially useful in a stellarator plasma where core E_r is important to understand bulk and impurity transport. This method also allows one to differentiate between Pfirsch–Schlüter and bootstrap flows.

Acknowledgments

The authors would like to thank the HSX team for machine operation and Jason Smoniewski for SFINCS code results. This material is based upon work supported by the U.S. Department of Energy, Office of Science, Office of Fusion Energy Science under award number DE-FG02-93ER54222. Data for figures included in this publication are available for access at http://hsx.wisc.edu/HSXPublicationData

References

[1] Mynick H.E. and Hitchon W.N.G. 1983 Effect of the ambipolar potential on stellarator confinement *Nucl. Fusion* **23** 1053
[2] Burhenn R. *et al* 2009 On impurity handling in high performance stellarator/heliotron plasmas *Nucl. Fusion* **49** 065005
[3] Watanabe K.Y., Nakajima N., Okamoto M., Yamazaki K., Nakamura Y. and Wakatani M. 1995 Effect of collisionality and radial electric field on bootstrap current in the large helical device *Nucl. Fusion* **35** 335
[4] Schmitt J.C., Talmadge J.N., Anderson D.T. and Hanson J.D. 2014 Modeling, measurement, and 3D equilibrium reconstruction of the bootstrap current in the helically symmetric experiment *Phys. Plasmas* **21** 092518
[5] Briesemeister A., Zhai K., Anderson D.T., Anderson F.S.B., Lore J. and Talmadge J.N. 2010 Flow velocity measurements using CHERS in the HSX stellarator *Contrib. Plasma Phys.* **50** 741–4
[6] Briesemeister A., Zhai K., Anderson D.T., Anderson F.S.B. and Talmadge J.N. 2013 Comparison of the flows and radial electric field in the HSX stellarator to neoclassical calculations *Plasma Phys. Control. Fusion* **55** 014002
[7] Arévalo J., Alonso J.A., McCarthy K.J. and Velasco J.L. 2013 Incompressibility of impurity flows in low density TJ-II plasmas and comparison with neoclassical theory *Nucl. Fusion* **53** 023003
[8] Arévalo J., Alonso J.A., McCarthy K.J., Velasco J.L., García-Regaña J.M. and Landreman M. 2014 Compressible impurity flow in the TJ-II stellarator *Nucl. Fusion* **54** 013008
[9] Schmitt J.C., Talmadge J.N. and Anderson D.T. 2013 Measurement of a helical Pfirsch–Schlüter current with reduced magnitude in HSX *Nucl. Fusion* **53** 082001
[10] Nemov V.V. 1988 Calculations of the magnetic surface function gradient and associated quantities in a torsatron *Nucl. Fusion* **28** 1727
[11] Nemov V.V. 1990 An investigation of Pfirsch–Schlüter currents in an $l = 2$ torsatron *Nucl. Fusion* **30** 927
[12] Anderson D.T. *et al* 2006 Overview of recent results from HSX *Fusion Sci. Technol.* **50** 171

[13] Canik J.M., Anderson D.T., Anderson F.S.B., Likin K.M., Talmadge J.N. and Zhai K. 2007 Experimental demonstration of improved neoclassical transport with quasihelical symmetry *Phys. Rev. Lett.* **98** 085002
[14] Dobbins T.J., Kumar S.T.A. and Anderson D.T. 2016 A synthetic diagnostic for beam emission spectroscopy in the helically symmetric experiment stellarator *Rev. Sci. Instrum.* **87** 11D413
[15] Spong D.A. 2005 Generation and damping of neoclassical plasma flows in stellarators *Phys. Plasmas* **12** 056114
[16] Lore J., Guttenfelder W., Briesemeister A., Anderson D.T., Anderson F.S.B., Deng C.B., Likin K.M., Spong D.A., Talmadge J.N. and Zhai K. 2010 Internal electron transport barrier due to neoclassical ambipolarity in the helically symmetric experiment *Phys. Plasmas* **17** 056101
[17] Summers H.P. 2004 The ADAS user manual version 2.6
[18] Helander P. 2014 Theory of plasma confinement in non-axisymmetric magnetic fields *Rep. Prog. Phys.* **77** 087001
[19] Landreman M. 2011 The monoenergetic approximation in stellarator neoclassical calculations *Plasma Phys. Control. Fusion* **53** 082003
[20] Pütterich T., Viezzer E., Dux R., McDermott R.M. and The ASDEX Upgrade Team 2012 Poloidal asymmetry of parallel rotation measured in ASDEX Upgrade *Nucl. Fusion* **52** 083013
[21] Marr K.D., Lipschultz B., Catto P.J., McDermott R.M., Reinke M.L. and Simakov A.N. 2010 Comparison of neoclassical predictions with measured flows and evaluation of a poloidal impurity density asymmetry *Plasma Phys. Control. Fusion* **52** 055010
[22] Helander P. 1998 Bifurcated neoclassical particle transport *Phys. Plasmas* **5** 3999–4004
[23] Pedrosa M.A., Alonso J.A., García-Regaña J.M., Hidalgo C., Velasco J.L., Calvo I., Kleiber R., Silva C. and Helander P. 2015 Electrostatic potential variations along flux surfaces in stellarators *Nucl. Fusion* **55** 052001
[24] García-Regaña J.M., Kleiber R., Beidler C.D., Turkin Y., Maaßberg H. and Helander P. 2013 On neoclassical impurity transport in stellarator geometry *Plasma Phys. Control. Fusion* **55** 074008
[25] Landreman M., Smith H.M., Moll A. and Helander P. 2014 Comparison of particle trajectories and collision operators for collisional transport in nonaxisymmetric plasmas *Phys. Plasmas* **21** 042503